Letter | Editors' Suggestion

Origin of charge density wave in the kagome metal CsV_3Sb_5 as revealed by optical spectroscopy

Xiaoxiang Zhou,[1,*] Yongkai Li,[2,3,*] Xinwei Fan,[1,*] Jiahao Hao,[1] Yaomin Dai,[1,†] Zhiwei Wang,[2,3,‡] Yugui Yao,[2,3] and Hai-Hu Wen[1,§]

[1]*National Laboratory of Solid State Microstructures and Department of Physics, Collaborative Innovation Center of Advanced Microstructures, Nanjing University, Nanjing 210093, China*

[2]*Key Laboratory of Advanced Optoelectronic Quantum Architecture and Measurement (MOE), School of Physics, Beijing Institute of Technology, Beijing 100081, China*

[3]*Beijing Key Lab of Nanophotonics and Ultrafine Optoelectronic Systems, Beijing Institute of Technology, Beijing 100081, China*

(Received 5 April 2021; accepted 21 June 2021; published 2 July 2021)

We report on a study of the optical properties of CsV_3Sb_5 for a large number of temperatures above and below the charge-density-wave (CDW) transition. Above the CDW transition, the low-frequency optical conductivity reveals two Drude components with distinct widths. An examination of the band structure allows us to ascribe the narrow Drude component to a light-electron-like and multiple Dirac bands, and the broad Drude component to heavy-hole bands near the M points which form saddle points near the Fermi level. Upon entering the CDW state, the opening of the CDW gap is clearly observed. A large portion of the broad Drude component is removed by the gap, whereas the narrow Drude component is not affected. Meanwhile, an absorption peak associated with interband transitions involving the saddle points shifts to higher energy and grows in weight. These observations attest to the importance of saddle point nesting in driving the CDW instability in CsV_3Sb_5.

DOI: 10.1103/PhysRevB.104.L041101

The kagome lattice has long served as a fertile ground for exploring exotic physics because it supports a wide variety of intriguing topological states and electronic instabilities. For example, electrons in a kagome lattice usually form flat bands and symmetry-protected Dirac points, giving rise to various interesting quantum phenomena associated with nontrivial band topology [1–6]. Furthermore, depending on the electron filling, on-site repulsion U, and nearest-neighbor Coulomb interaction V, the ground state of a kagome lattice system can be a quantum spin liquid [7,8], charge bond order [9,10], superconductor [9–12], charge density wave (CDW) [9], or spin density wave (SDW) [12].

Recently, a new family of kagome metals, AV_3Sb_5 (A = K, Rb, or Cs), was discovered [13], prompting an intense exploration of the exotic physics in these compounds [14–33]. Superconductivity with a transition temperature T_c of 0.93, 0.92, and 2.5 K has been reported in KV_3Sb_5, RbV_3Sb_5, and CsV_3Sb_5, respectively [14–16]. By applying pressure, T_c of CsV_3Sb_5 can be enhanced to about 8 K at 2 GPa [17,18]. While an ultralow-temperature thermal transport study has revealed possible nodal superconductivity in CsV_3Sb_5 [19], magnetic penetration depth and specific heat measurements have provided evidence of nodeless superconducting gaps [20]. In addition to superconductivity, AV_3Sb_5 undergoes a CDW transition at T_{CDW} = 78, 103, and 94 K for A = K, Rb, and Cs, respectively [13–16]. X-ray diffraction [14] and scanning tunneling microscopy (STM) [21–23] measurements have revealed a 2×2 superlattice, attesting to the formation of charge ordering. Moreover, the giant anomalous Hall effect [24,25] and multiple topologically protected Dirac bands near the Fermi level E_F [14,16] have also been observed in these compounds.

Although some experimental results have demonstrated that the CDW order has a strong influence on superconductivity and nontrivial topological bands [17,19,23,25], the driving mechanism of the CDW order remains unclear. Theoretical calculations suggested that the CDW transition is driven by the Peierls instability related to the Fermi surface (FS) nesting and the softening of an acoustic phonon mode [29], which is supported by STM measurements [21,23], but on the other hand, a hard x-ray scattering study on RbV_3Sb_5 and CsV_3Sb_5 failed to detect the expected acoustic phonon anomaly at the CDW wave vector, pointing to an unconventional electronic-driven mechanism [28].

In this Letter, we investigate the optical properties of CsV_3Sb_5 at 15 temperatures above and below T_{CDW}. Two Drude components (a narrow one and a broad one) yield a good description of the low-frequency optical conductivity. Through close inspection of the band structure, we ascribe the narrow Drude component to a light-electron-like and multiple Dirac bands and the broad Drude component to heavy-hole bands near the M points which have saddle points near E_F. Below T_{CDW}, the optical conductivity clearly demonstrates the formation of the CDW gap, which significantly suppresses the weight of the broad Drude component but does not have a noticeable effect on the narrow Drude component. Simultaneously, interband transitions involving states near the saddle points are enhanced and shift to higher energy. These

*These authors contributed equally to this work.
†ymdai@nju.edu.cn
‡zhiweiwang@bit.edu.cn
§hhwen@nju.edu.cn

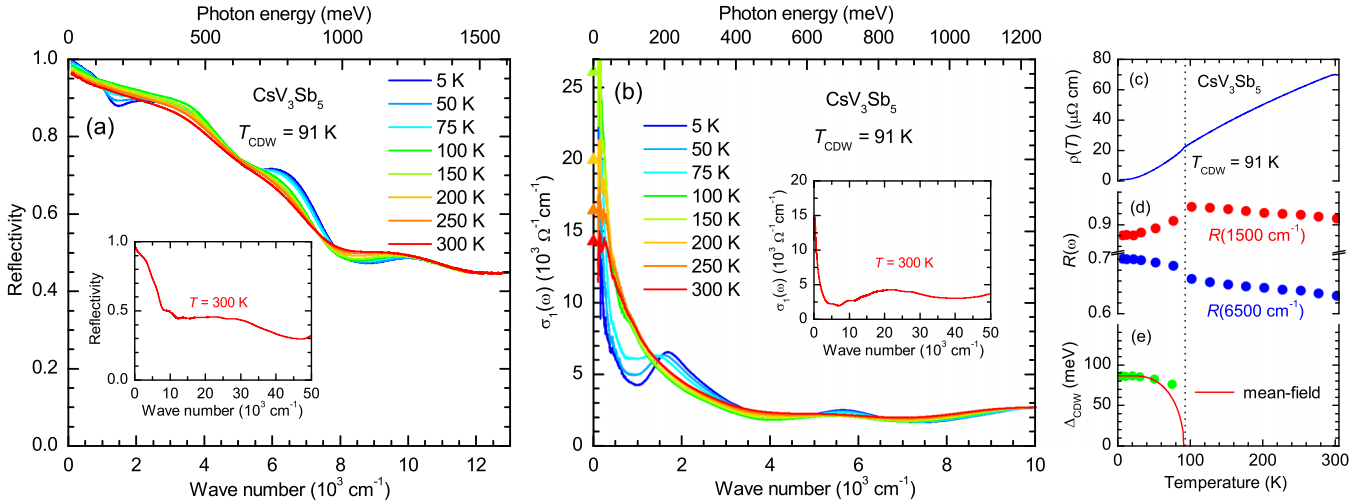

FIG. 1. (a) and (b) show the reflectivity $R(\omega)$ and the real part of the optical conductivity $\sigma_1(\omega)$ of CsV_3Sb_5, respectively, at several representative temperatures above and below T_{CDW}. The insets of (a) and (b) display $R(\omega)$ and $\sigma_1(\omega)$ up to 50 000 cm^{-1} at 300 K, respectively. The solid triangles on the y axis of (b) denote the dc conductivity at different temperatures obtained from transport measurements. (c) The T-dependent resistivity $\rho(T)$ of CsV_3Sb_5. (d) The T dependence of $R(\omega)$ at $\omega = 1500$ cm^{-1} (red solid circles) and $\omega = 6500$ cm^{-1} (blue solid circles). (e) The CDW gap Δ_{CDW} at different temperatures (green solid circles) and the BCS mean-field behavior (red solid curve).

experimental results are in favor of the scenario that nesting of the saddle points at M induces the CDW instability in CsV_3Sb_5.

Single crystals of CsV_3Sb_5 were synthesized via a self-flux method [13]. Figure 1(c) shows the T-dependent resistivity $\rho(T)$ of our sample, which exhibits a CDW transition at $T_{CDW} = 91$ K. The *ab*-plane reflectivity $R(\omega)$ of CsV_3Sb_5 was measured at a near-normal angle of incidence on a newly cleaved surface using a Bruker Vertex 80V Fourier transform spectrometer equipped with an *in situ* gold evaporation technique [34]. Data in the frequency range of 100–12 000 cm^{-1} were collected at 15 temperatures from 300 down to 5 K. Then, an AvaSpec-2048×14 optical fiber spectrometer was employed to extend $R(\omega)$ to 50 000 cm^{-1} at room temperature. The real part of the optical conductivity $\sigma_1(\omega)$ was obtained from a Kramers-Kronig analysis of the measured $R(\omega)$ [35].

Figure 1(a) displays $R(\omega)$ of CsV_3Sb_5 at several representative temperatures above and below T_{CDW} up to 13 000 cm^{-1}; the inset shows $R(\omega)$ at 300 K up to 50 000 cm^{-1}. Above T_{CDW}, $R(\omega)$ approaches unity in the low-frequency limit and increases with decreasing T in the far-infrared range, agreeing well with the metallic nature of this compound. Below T_{CDW}, for example, at 5 K (blue curve), a dramatic suppression of $R(\omega)$ develops at about 1500 cm^{-1} alongside a humplike feature at about 6500 cm^{-1}. The evolution of $R(1500\,\text{cm}^{-1})$ and $R(6500\,\text{cm}^{-1})$ with T is traced out in Fig. 1(d). Both the suppression of $R(1500\,\text{cm}^{-1})$ and the enhancement of $R(6500\,\text{cm}^{-1})$ occur at T_{CDW}, suggesting that they are intimately related to the CDW transition.

More straightforward information can be obtained from $\sigma_1(\omega)$, as it is directly linked to the joint density of states [36]. Figure 1(b) shows $\sigma_1(\omega)$ of CsV_3Sb_5 at different temperatures above and below T_{CDW}. The solid triangles on the y axis denote the dc conductivity σ_{dc} at different temperatures obtained from transport measurements, which agrees quite well with the zero-frequency extrapolation of $\sigma_1(\omega)$. For $T > T_{CDW}$, the low-frequency $\sigma_1(\omega)$ exhibits a pronounced Drude response, i.e., a peak centered at zero frequency, which is a typical characteristic of metals. As T is lowered, the Drude peak narrows, reflecting the reduction of the quasiparticle scattering rate. In the high-frequency range, two broad bands associated with interband transitions can be resolved at about 5500 and 10 000 cm^{-1}. For $T < T_{CDW}$, $\sigma_1(\omega)$ below about 1500 cm^{-1} is significantly suppressed, and the lost spectral weight [the area under $\sigma_1(\omega)$] is transferred to a higher frequency range 1500–4000 cm^{-1}, resulting in a conspicuous peak at about 1700 cm^{-1}. This gives strong optical evidence of the opening of a density-wave gap [37–39]. The gap value Δ_{CDW} can be determined from the crossing point between $\sigma_1(\omega)$ at $T < T_{CDW}$ and that at T slightly above T_{CDW}, such as 100 K. At 5 K, $\Delta_{CDW} = 86.5$ meV, which gives $2\Delta_{CDW}/k_B T_{CDW} \simeq 22$, a ratio much larger than the weak-coupling BCS value of 3.53. This large ratio implies that the CDW in CsV_3Sb_5 is unlikely to be driven by the conventional weak-coupling electron-phonon interaction [40]; a strong-coupling mechanism may be involved [41]. The green solid circles in Fig. 1(e) denote Δ_{CDW} at different temperatures. In the proximity of T_{CDW}, Δ_{CDW} deviates from the BCS mean-field T dependence (red solid curve) for $\Delta_0 = 86.5$ meV and $T_{CDW} = 91$ K, indicating an unconventional CDW in CsV_3Sb_5. This behavior is consistent with a recent study on KV_3Sb_5 [30]. Furthermore, the residual Drude peak in the low-frequency range becomes extremely narrow, while the band at about 5500 cm^{-1} intensifies and shifts to higher frequency.

In order to quantitatively analyze the optical data, we fit the measured $\sigma_1(\omega)$ to the Drude-Lorentz model,

$$\sigma_1(\omega) = \frac{2\pi}{Z_0}\left[\sum_k \frac{\omega_{p,k}^2}{\tau_k\left(\omega^2 + \tau_k^{-2}\right)} \sum_j \frac{\gamma_j \omega^2 \omega_{p,j}^2}{\left(\omega_{0,j}^2 - \omega^2\right)^2 + \gamma_j^2 \omega^2}\right], \quad (1)$$

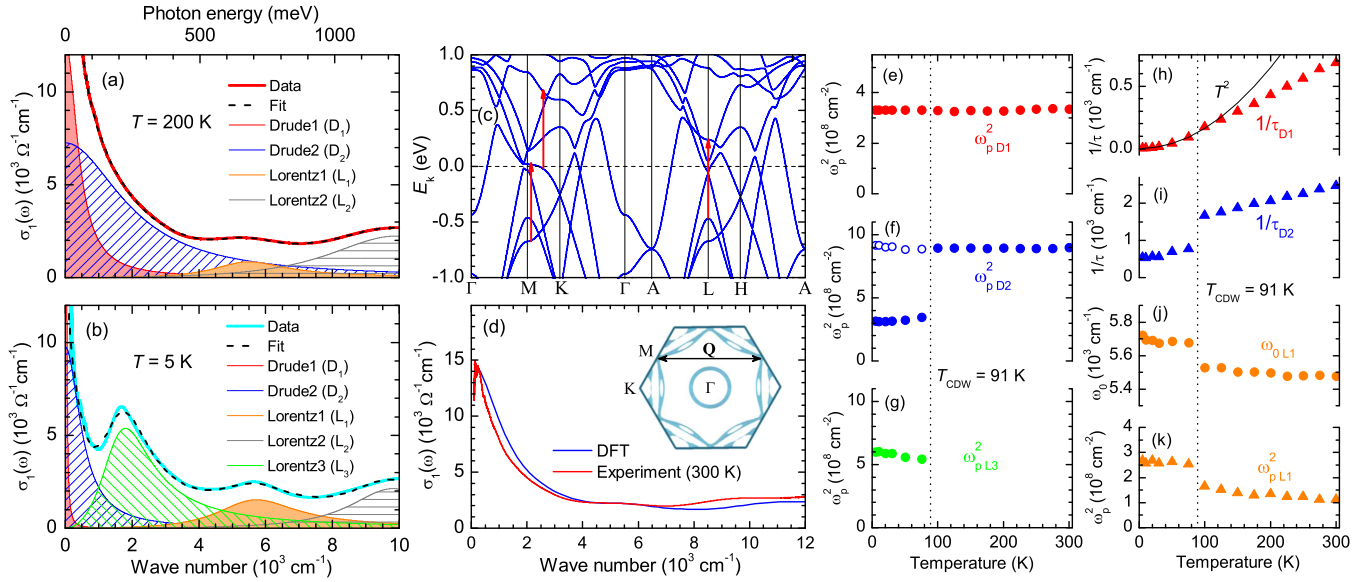

FIG. 2. (a) The red solid curve is $\sigma_1(\omega)$ for CsV_3Sb_5 measured at 200 K. The black dashed line through the data represents the Drude-Lorentz fit, which is decomposed into a narrow Drude component D_1 (red shaded area), a broad Drude component D_2 (blue hatched area), and two Lorentz components, L_1 and L_2, denoted by the orange shaded and gray hatched regions, respectively. (b) The measured $\sigma_1(\omega)$ at 5 K (cyan solid curve) and the fit (black dashed curve). In addition to the components used for the fit at 200 K, an extra Lorentz component, L_3 (green hatched area), is required to describe the opening of the CDW gap. (c) The calculated band structure for CsV_3Sb_5. (d) The calculated $\sigma_1(\omega)$ for CsV_3Sb_5 (blue curve), which is compared to the measured $\sigma_1(\omega)$ at 300 K (red curve). Inset: The calculated Fermi surface of CsV_3Sb_5 projected to the k_x-k_y plane; the arrow denotes the nesting vector **Q**. (e)–(k) The T dependence of the parameters extracted from the Drude-Lorentz fit.

where $Z_0 \simeq 377\ \Omega$ is the impedance of free space. The first term is a sum of free-carrier Drude responses. Each response is characterized by a plasma frequency ω_p, with ω_p^2 being proportional to the carrier density, and a scattering rate $1/\tau$ describing the width of the Drude profile at half maximum. In the second term, $\omega_{0,j}$, γ_j, and $\omega_{p,j}$ correspond to the resonance frequency, linewidth, and plasma frequency (strength) of the j_{th} Lorentz oscillator, respectively. The red solid curve in Fig. 2(a) is the measured $\sigma_1(\omega)$ at 200 K, and the dashed line through the data represents the fitting result, which is the superposition of a narrow Drude component D_1 (red shaded area), a broad Drude component D_2 (blue hatched area), and two Lorentz components, L_1 and L_2 (the orange shaded and grey hatched areas, respectively).

To ascertain the origin of the components in $\sigma_1(\omega)$, we calculated the band structure, the FS, and the *ab*-plane $\sigma_1(\omega)$ of CsV_3Sb_5 within the density-functional-theory (DFT) framework implemented in the full-potential linearized augmented plane wave code WIEN2K [42–45]. Figure 2(c) displays the calculated band structure of CsV_3Sb_5, which is similar to previous calculations [13,14,29]. It is noteworthy that there are three types of bands crossing E_F: (i) a light-electron-like band near the Γ point, (ii) multiple Dirac bands with quasilinear dispersion near the K points, and (iii) heavy-hole-like bands with weak dispersion which form saddle points near E_F at M. The inset in Fig. 2(d) shows the calculated FS of CsV_3Sb_5 projected to the k_x-k_y plane. The circle around the center of the Brillouin zone denotes a cylinderlike Fermi pocket produced by the light-electron-like band near Γ; the multiple Dirac bands give rise to the FS sheets near K (between Γ and K), and the FSs near M (between M and K) are formed by the heavy-hole-like bands with saddle points near E_F. Figure 2(d) shows that the calculated $\sigma_1(\omega)$ (blue solid curve) agrees quite well with the experimental $\sigma_1(\omega)$ (red solid curve).

Previous optical studies on Dirac or Weyl semimetals have shown that the Drude response associated with Dirac bands is very narrow [46–49], and the small scattering rate in these materials has been proved to stem from a protection mechanism that strongly suppresses backscattering [50–52]. A recent optical study on RhSi has corroborated that light-electron bands give rise to a narrow Drude component, while heavy-hole bands produce a broad Drude component [53]. Furthermore, saddle points near E_F act as scattering sinks, which lead to a large quasiparticle scattering rate [54]. Based on these facts, it is reasonable to attribute D_1 to the light-electron-like and multiple Dirac bands and to ascribe D_2 to the heavy-hole bands having saddle points near E_F at the M points. L_1 and L_2 are associated with interband transitions. The energy of the interband transitions involving states near the saddle points at M and L, as indicated by the red arrows in Fig. 2(c), exactly matches the resonance frequency, namely, the peak position (∼0.7 eV), of L_1. This match allows us to link L_1 to interband transitions involving the saddle points at M and L. Here, we would like to point out that interband transitions between other bands may also contribute to L_1, but those involving the saddle points at M and L are expected to dominate because near the saddle points, the density of states (DOS) is greatly enhanced due to the flatness of the bands.

Having elaborated the origin of each component, we examine $\sigma_1(\omega)$ in the CDW state and the evolution of the optical

response with T. Figure 2(b) depicts $\sigma_1(\omega)$ of CsV_3Sb_5 at 5 K (cyan solid curve) and the fitting result (black dashed curve). Due to the opening of the CDW gap, D_2 is significantly suppressed, and a third Lorentz component, L_3 (green hatched region), is introduced to describe the gap feature in $\sigma_1(\omega)$. The same approach has been used to describe the SDW gap in iron pnictides [39,55,56]. Moreover, D_1 becomes very narrow to account for the extremely small $\rho(T)$ at 5 K; L_1 grows in spectral weight and shifts to higher frequency. In order to track the detailed T dependence of the optical properties for CsV_3Sb_5, we apply the Drude-Lorentz fit to $\sigma_1(\omega)$ at all 15 measured temperatures, which returns the T dependence of the parameters for all components. To achieve more accurate fits, the constraint condition $\sigma_1(\omega \to 0) \equiv 1/\rho(T)$ has been applied for the fit at all temperatures.

The T dependence of ω^2_{p,D_1} and ω^2_{p,D_2} is traced out in Figs. 2(e) and 2(f), respectively. Above $T_{\rm CDW}$, neither ω^2_{p,D_1} nor ω^2_{p,D_2} exhibits observable T dependence, indicating no change of the FSs. Upon entering the CDW state, while ω^2_{p,D_1} remains unchanged, a sharp drop in ω^2_{p,D_2} is observed. This behavior suggests that the FSs associated with the light-electron-like and Dirac bands are not affected by the CDW transition, whereas a large portion (about 65%) of the FSs formed by the heavy-hole bands with saddle points at M is removed due to the formation of the CDW gap. The lost spectral weight from D_2 is transferred to higher energy. In order to locate the spectral weight, we plot ω^2_{p,L_3} as a function of T in Fig. 2(g). It is immediately obvious that the value of ω^2_{p,L_3} is approximately equal to the decrease of ω^2_{p,D_2}, and ω^2_{p,L_3} exhibits the T dependence opposite to ω^2_{p,D_2}, implying that the lost spectral weight from D_2 is most likely transferred to L_3. To verify this assertion, $\omega^2_{p,D_2} + \omega^2_{p,L_3}$ is plotted as open circles in Fig. 2(f), which reveals that $\omega^2_{p,D_2} + \omega^2_{p,L_3}$ in the CDW state has the same value as ω^2_{p,D_2} above $T_{\rm CDW}$. This result strongly suggests that the lost spectral weight from D_2 is fully captured by L_3, consistent with the expected behavior for a density-wave gap [37,38]. Moreover, the conservation of the spectral weight between D_2 and L_3 further confirms that the CDW transition bears no influence on ω^2_{p,D_1}.

Figures 2(h) and 2(i) display $1/\tau_{D_1}$ and $1/\tau_{D_2}$, respectively. Both diminish linearly with decreasing T above $T_{\rm CDW}$. No abrupt change in $1/\tau_{D_1}$ is observed at $T_{\rm CDW}$, again hinting that the light-electron-like and Dirac bands are not involved in the CDW transition. In the low-temperature range, $1/\tau_{D_1}$ follows Fermi-liquid T^2 dependence, as depicted by the solid curve in Fig. 2(h), in accord with the expected behavior for bands with Dirac-like dispersion [46,57]. In contrast, a sudden drop in $1/\tau_{D_2}$ occurs at $T_{\rm CDW}$, suggesting that the quasiparticle scattering in the heavy-hole bands with saddle points near E_F is also altered by the formation of the CDW gap.

The evolution of L_1 is portrayed in Figs. 2(j) and 2(k). Both the resonance frequency ω_{0,L_1} and the intensity ω^2_{p,L_1} of L_1 exhibit a jump at $T_{\rm CDW}$. While the interband transitions at L involve bands far away from $E_{\rm F}$, which is unlikely to be affected by the CDW transition, the opening of the CDW gap in the heavy-hole bands with saddle points near E_F at M can account for the behavior of L_1. Upon the CDW transition, the DOS near E_F is depleted, leading to the formation of the CDW gap near M. The removed DOS is retrieved just above the gap energy, resulting in a pileup of the DOS near the gap edge. This DOS pileup not only shifts the interband transitions towards higher energy, accounting for the jump in ω_{0,L_1}, but also enhances their intensity due to the enhancement of DOS, which explains the increase of ω^2_{p,L_1}.

Our experimental results provide important information for understanding the driving mechanism of the CDW order. Recent theoretical calculations [29] suggested a 2×2 CDW with an inverse star of David pattern as the ground state of AV_3Sb_5 and also proposed that the CDW is induced by the Peierls instability related to the FS nesting and the softening of a breathing phonon mode of V atoms. The calculated phonon band structure shows a softening of acoustic phonon modes near the M and L points of the Brillouin zone, indicating a strong instability. The q vector of the soft mode at M coincides with the nesting vector between neighboring saddle points at M. Consequently, the CDW instability significantly reduces the DOS at E_F by suppressing the saddle points at M, which leads to the formation of the CDW gap in the heavy bands near the M points. Assuming an electronically driven charge order and FS nesting effect, another theoretical work [27] obtained a star of David CDW with orbital currents for AV_3Sb_5, and the resulting band structure also exhibits a gap opening around the M points. Although it is still controversial whether the FS nesting driving mechanism for a CDW in one-dimensional systems can be applied to two-dimensional materials [58], Rice and Scott have demonstrated that in a two-dimensional system, the nesting of saddle points near $E_{\rm F}$, which is not the usual FS nesting, is unstable against CDW formation [54].

AV_3Sb_5 has saddle points near $E_{\rm F}$ at the M points [13,14,29,59–61], and these saddle points are connected by the nesting vector $\mathbf{Q}$, as shown in the inset in Fig. 2(d). Our experimental observations, i.e., the strong suppression of ω^2_{p,D_2}, the shift of $\omega_{0,L1}$ to higher energy, and the increase of $\omega^2_{p,L1}$ upon the CDW transition, point to the formation of a CDW gap in the heavy bands having saddle points near E_F at M. The strong momentum dependence of the CDW gap has been confirmed by recent angle-resolved photoemission spectroscopy measurements [59–61]. The opening of the CDW gap in the heavy bands with saddle points at M suggests that nesting of the saddle points at M may play an important role in driving the CDW instability in CsV_3Sb_5.

To summarize, the optical properties of CsV_3Sb_5 have been examined at numerous temperatures between 5 and 300 K. Above $T_{\rm CDW}$, the optical conductivity can be well described by two Drude components: a narrow one and a broad one. An investigation into the calculated band structure suggests that the narrow Drude component is associated with a light-electron-like and multiple Dirac bands, while the broad Drude component arises from heavy-hole bands with saddle points near E_F at M. Below $T_{\rm CDW}$, the opening of the CDW gap is clearly observed in $\sigma_1(\omega)$. The spectral weight of the broad Drude component is substantially suppressed by the gap, while the narrow Drude component remains unchanged. In addition, interband transitions that involve the electronic states near the saddle points at M gain some weight and shift to higher energy. These observations signify that the CDW

instability in CsV_3Sb_5 is intimately related to the nesting of the saddle points at M.

We thank S. L. Yu, Q. H. Wang, R. Thomale, B. H. Yan, H. Miao, B. Xu, R. Yang, and J. B. Qi for helpful discussions. We gratefully acknowledge financial support from the National Key R&D Program of China (Grants No. 2016YFA0300401 and No. 2020YFA0308800), the National Natural Science Foundation of China (Grants No. 11874206, No.12061131001, No. 92065109, No. 11734003, and No. 11904294), the Fundamental Research Funds for the Central Universities (Grant No. 020414380095), the Jiangsu Shuangchuang program, the Beijing Natural Science Foundation (Grant No. Z190006), and the Beijing Institute of Technology Research Fund Program for Young Scholars (Grant No. 3180012222011). Z.W. would like to thank Micronano Center at BIT for the assistance of sample characterization.

[1] H.-M. Guo and M. Franz, Phys. Rev. B **80**, 113102 (2009).
[2] I. I. Mazin, H. O. Jeschke, F. Lechermann, H. Lee, M. Fink, R. Thomale, and R. Valentí, Nat. Commun. **5**, 4261 (2014).
[3] L. Ye, M. Kang, J. Liu, F. von Cube, C. R. Wicker, T. Suzuki, C. Jozwiak, A. Bostwick, E. Rotenberg, D. C. Bell, L. Fu, R. Comin, and J. G. Checkelsky, Nature (London) **555**, 638 (2018).
[4] M. Kang, L. Ye, S. Fang, J.-S. You, A. Levitan, M. Han, J. I. Facio, C. Jozwiak, A. Bostwick, E. Rotenberg *et al.*, Nat. Mater. **19**, 163 (2020).
[5] Z. Liu, M. Li, Q. Wang, G. Wang, C. Wen, K. Jiang, X. Lu, S. Yan, Y. Huang, D. Shen, J.-X. Yin, Z. Wang, Z. Yin, H. Lei, and S. Wang, Nat. Commun. **11**, 4002 (2020).
[6] J.-X. Yin, S. S. Zhang, G. Chang, Q. Wang, S. S. Tsirkin, Z. Guguchia, B. Lian, H. Zhou, K. Jiang, I. Belopolski, N. Shumiya, D. Multer, M. Litskevich, T. A. Cochran, H. Lin, Z. Wang, T. Neupert, S. Jia, H. Lei, and M. Z. Hasan, Nat. Phys. **15**, 443 (2019).
[7] L. Balents, Nature (London) **464**, 199 (2010).
[8] S. Yan, D. A. Huse, and S. R. White, Science **332**, 1173 (2011).
[9] W.-S. Wang, Z.-Z. Li, Y.-Y. Xiang, and Q.-H. Wang, Phys. Rev. B **87**, 115135 (2013).
[10] M. L. Kiesel, C. Platt, and R. Thomale, Phys. Rev. Lett. **110**, 126405 (2013).
[11] W.-H. Ko, P. A. Lee, and X.-G. Wen, Phys. Rev. B **79**, 214502 (2009).
[12] S.-L. Yu and J.-X. Li, Phys. Rev. B **85**, 144402 (2012).
[13] B. R. Ortiz, L. C. Gomes, J. R. Morey, M. Winiarski, M. Bordelon, J. S. Mangum, I. W. H. Oswald, J. A. Rodriguez-Rivera, J. R. Neilson, S. D. Wilson, E. Ertekin, T. M. McQueen, and E. S. Toberer, Phys. Rev. Mater. **3**, 094407 (2019).
[14] B. R. Ortiz, S. M. L. Teicher, Y. Hu, J. L. Zuo, P. M. Sarte, E. C. Schueller, A. M. M. Abeykoon, M. J. Krogstad, S. Rosenkranz, R. Osborn, R. Seshadri, L. Balents, J. He, and S. D. Wilson, Phys. Rev. Lett. **125**, 247002 (2020).
[15] B. R. Ortiz, P. M. Sarte, E. M. Kenney, M. J. Graf, S. M. L. Teicher, R. Seshadri, and S. D. Wilson, Phys. Rev. Mater. **5**, 034801 (2021).
[16] Q. Yin, Z. Tu, C. Gong, Y. Fu, S. Yan, and H. Lei, Chin. Phys. Lett. **38**, 037403 (2021).
[17] K. Y. Chen, N. N. Wang, Q. W. Yin, Y. H. Gu, K. Jiang, Z. J. Tu, C. S. Gong, Y. Uwatoko, J. P. Sun, H. C. Lei, J. P. Hu, and J.-G. Cheng, Phys. Rev. Lett. **126**, 247001 (2021).
[18] X. Chen, X. Zhan, X. Wang, J. Deng, X.-B. Liu, X. Chen, J.-G. Guo, and X. Chen, Chin. Phys. Lett. **38**, 057402 (2021).
[19] C. C. Zhao, L. S. Wang, W. Xia, Q. W. Yin, J. M. Ni, Y. Y. Huang, C. P. Tu, Z. C. Tao, Z. J. Tu, C. S. Gong, H. C. Lei, Y. F. Guo, X. F. Yang, and S. Y. Li, arXiv:2102.08356.
[20] W. Duan, Z. Nie, S. Luo, F. Yu, B. R. Ortiz, L. Yin, H. Su, F. Du, A. Wang, Y. Chen, X. Lu, J. Ying, S. D. Wilson, X. Chen, Y. Song, and H. Yuan, arXiv:2103.11796.
[21] H. Chen, H. Yang, B. Hu, Z. Zhao, J. Yuan, Y. Xing, G. Qian, Z. Huang, G. Li, Y. Ye *et al.*, arXiv:2103.09188.
[22] Z. Liang, X. Hou, W. Ma, F. Zhang, P. Wu, Z. Zhang, F. Yu, J. J. Ying, K. Jiang, L. Shan, Z. Wang, and X.-H. Chen, arXiv:2103.04760.
[23] Y.-X. Jiang, J.-X. Yin, M. M. Denner, N. Shumiya, B. R. Ortiz, J. He, X. Liu, S. S. Zhang, G. Chang, I. Belopolski *et al.*, arXiv:2012.15709.
[24] S.-Y. Yang, Y. Wang, B. R. Ortiz, D. Liu, J. Gayles, E. Derunova, R. Gonzalez-Hernandez, L. Šmejkal, Y. Chen, S. S. P. Parkin, S. D. Wilson, E. S. Toberer, T. McQueen, and M. N. Ali, Sci. Adv. **6**, eabb6003 (2020).
[25] F. H. Yu, T. Wu, Z. Y. Wang, B. Lei, W. Z. Zhuo, J. J. Ying, and X. H. Chen, arXiv:2102.10987.
[26] X. Feng, K. Jiang, Z. Wang, and J. Hu, arXiv:2103.07097.
[27] M. M. Denner, R. Thomale, and T. Neupert, arXiv:2103.14045.
[28] H. X. Li, T. T. Zhang, Y.-Y. Pai, C. Marvinney, A. Said, T. Yilmaz, Q. Yin, C. Gong, Z. Tu, E. Vescovo, R. G. Moore, S. Murakami, H. C. Lei, H. N. Lee, B. Lawrie, and H. Miao, arXiv:2103.09769.
[29] H. Tan, Y. Liu, Z. Wang, and B. Yan, arXiv:2103.06325.
[30] E. Uykur, B. R. Ortiz, S. D. Wilson, M. Dressel, and A. A. Tsirlin, arXiv:2103.07912.
[31] Z. Zhang, Z. Chen, Y. Zhou, Y. Yuan, S. Wang, J. Wang, H. Yang, C. An, L. Zhang, X. Zhu, Y. Zhou, X. Chen, J. Zhou, and Z. Yang, Phys. Rev. B **103**, 224513 (2021).
[32] H. Zhao, H. Li, B. R. Ortiz, S. M. L. Teicher, T. Park, M. Ye, Z. Wang, L. Balents, S. D. Wilson, and I. Zeljkovic, arXiv:2103.03118.
[33] J. Zhao, W. Wu, Y. Wang, and S. A. Yang, Phys. Rev. B **103**, L241117 (2021).
[34] C. C. Homes, M. Reedyk, D. A. Cradles, and T. Timusk, Appl. Opt. **32**, 2976 (1993).
[35] M. Dressel and G. Grüner, *Electrodynamics of Solids* (Cambridge University Press, Cambridge, 2002).
[36] D. N. Basov and T. Timusk, Rev. Mod. Phys. **77**, 721 (2005).
[37] L. Degiorgi, M. Dressel, A. Schwartz, B. Alavi, and G. Grüner, Phys. Rev. Lett. **76**, 3838 (1996).
[38] Z.-T. Zhu, J. L. Musfeldt, Z. S. Teweldemedhin, and M. Greenblatt, Phys. Rev. B **65**, 214519 (2002).
[39] W. Z. Hu, J. Dong, G. Li, Z. Li, P. Zheng, G. F. Chen, J. L. Luo, and N. L. Wang, Phys. Rev. Lett. **101**, 257005 (2008).
[40] G. Grüner, Rev. Mod. Phys. **60**, 1129 (1988).
[41] C. M. Varma and A. L. Simons, Phys. Rev. Lett. **51**, 138 (1983).
[42] P. Blaha, K. Schwarz, G. K. H. Madsen, D. Kvasnicka, and J.

Luitz, *WIEN2K, an Augmented Plane Wave + Local Orbitals Program for Calculating Crystal Properties* (Technische Universität Wien, Vienna, 2001).
[43] K. Schwarz and P. Blaha, Comput. Mater. Sci. **28**, 259 (2003).
[44] R. Abt, C. Ambrosch-Draxl, and P. Knoll, Phys. B (Amsterdam, Neth.) **194–196**, 1451 (1994).
[45] C. Ambrosch-Draxl and J. O. Sofo, Comput. Phys. Commun. **175**, 1 (2006).
[46] B. Xu, Y. M. Dai, L. X. Zhao, K. Wang, R. Yang, W. Zhang, J.Y. Liu, H. Xiao, G. F. Chen, A. J. Taylor, D.A. Yarotski, R. P. Prasankumar, and X. G. Qiu, Phys. Rev. B **93**, 121110(R) (2016).
[47] D. Neubauer, J. P. Carbotte, A. A. Nateprov, A. Löhle, M. Dressel, and A. V. Pronin, Phys. Rev. B **93**, 121202(R) (2016).
[48] M. B. Schilling, L. M. Schoop, B. V. Lotsch, M. Dressel, and A. V. Pronin, Phys. Rev. Lett. **119**, 187401 (2017).
[49] B. Xu, L. X. Zhao, P. Marsik, E. Sheveleva, F. Lyzwa, Y. M. Dai, G. F. Chen, X. G. Qiu, and C. Bernhard, Phys. Rev. Lett. **121**, 187401 (2018).
[50] T. Liang, Q. Gibson, M. N. Ali, M. Liu, R. J. Cava, and N. P. Ong, Nat. Mater. **14**, 280 (2015).
[51] T. Liang, J. Lin, Q. Gibson, T. Gao, M. Hirschberger, M. Liu, R. J. Cava, and N. P. Ong, Phys. Rev. Lett. **118**, 136601 (2017).
[52] N. Kumar, Y. Sun, N. Xu, K. Manna, M. Yao, V. Süss, I. Leermakers, O. Young, T. Förster, M. Schmidt, H. Borrmann, B. Yan, U. Zeitler, M. Shi, C. Felser, and C. Shekhar, Nat. Commun. **8**, 1642 (2017).
[53] Z. Ni, B. Xu, M.-A. Sánchez-Martínez, Y. Zhang, K. Manna, C. Bernhard, J. W. F. Venderbos, F. de Juan, C. Felser, A. G. Grushin, and L. Wu, npj Quantum Mater. **5**, 96 (2020).
[54] T. M. Rice and G. K. Scott, Phys. Rev. Lett. **35**, 120 (1975).
[55] M. Nakajima, S. Ishida, K. Kihou, Y. Tomioka, T. Ito, Y. Yoshida, C. H. Lee, H. Kito, A. Iyo, H. Eisaki, K. M. Kojima, and S. Uchida, Phys. Rev. B **81**, 104528 (2010).
[56] Y. M. Dai, A. Akrap, S. L. Bud'ko, P. C. Canfield, and C. C. Homes, Phys. Rev. B **94**, 195142 (2016).
[57] P. Hosur, S. A. Parameswaran, and A. Vishwanath, Phys. Rev. Lett. **108**, 046602 (2012).
[58] M. D. Johannes and I. I. Mazin, Phys. Rev. B **77**, 165135 (2008).
[59] Z. Wang, S. Ma, Y. Zhang, H. Yang, Z. Zhao, Y. Ou, Y. Zhu, S. Ni, Z. Lu, H. Chen, K. Jiang, L. Yu, Y. Zhang, X. Dong, J. Hu, H.-J. Gao, and Z. Zhao, arXiv:2104.05556.
[60] K. Nakayama, Y. Li, M. Liu, Z. Wang, T. Takahashi, Y. Yao, and T. Sato, arXiv:2104.08042.
[61] S. Cho, H. Ma, W. Xia, Y. Yang, Z. Liu, Z. Huang, Z. Jiang, X. Lu, J. Liu, Z. Liu, J. Jia, Y. Guo, J. Liu, and D. Shen, arXiv:2105.05117.